frontiers | Frontiers in Earth Science

TYPE Original Research
PUBLISHED 09 January 2023
DOI 10.3389/feart.2022.1012324

OPEN ACCESS

EDITED BY
Juan Teng,
Yangtze University, China

REVIEWED BY
Jianhua He,
Chengdu University of Technology, China
Saipeng Huang,
Northeast Petroleum University, China

*CORRESPONDENCE
Qiang Fu,
fuqiang@tongji.edu.cn

SPECIALTY SECTION
This article was submitted to Geochemistry, a section of the journal Frontiers in Earth Science

RECEIVED 05 August 2022
ACCEPTED 16 September 2022
PUBLISHED 09 January 2023

CITATION
Yang B, Fu Q, Liu J, Ma W and Zhao S (2023), Study on fault sealing of the Lishui West Sag in the East China Sea Basin.
Front. Earth Sci. 10:1012324.
doi: 10.3389/feart.2022.1012324

Study on fault sealing of the Lishui West Sag in the East China Sea Basin

Bing Yang[1], Qiang Fu[1]*, Jinshui Liu[2], Wenrui Ma[2] and Shijie Zhao[1]

[1]State Key Laboratory of Marine Geology, Tongji University, Shanghai, China, [2]Shanghai Branch Company of CNOOC (China) Ltd., Shanghai, China

The property of fault sealing is a critical controlling factor for hydrocarbon transportation. To date, the sealing property of the complex fault system in the Lishui West Sag is still not clear, meaning it is essential to study regional hydrocarbon transportation and reservoir formation. In this study, we use an integrated method to quantitatively analyze and characterize several important index parameters that affect the sealing property of the faults in the Lishui West Sag based on regional logs and seismic data. We calculated the shale smear factor (SSF), shale gouge ratio (SGR), and clay smear potential (CSP) to characterize the lateral sealing property of the main faults covered with the giant thick shale cap in the Lishui West Sag. We used the vertical shale smear factor Q to clarify the vertical sealing property of these faults quantitatively as a comparison. The results show that the shale cap has a strong smear ability in the Lishui West Sag, while the active fault could moderate the smear. A high fault activity in this area benefits hydrocarbon transportation at the same time. The lateral sealing property and the vertical sealing property of the main faults in the Lishui West Sag have negative correlations.

KEYWORDS

fault sealing, shale smear, quantitative evaluation, Lishui West Sag, East China Sea Basin

Introduction

Fault sealing has confused geologists in reservoir theory and exploration practice, who have tried to evaluate the fault sealing property since the 1960s. Smith (1966) established a model of sand–clay docking to clarify sealing and non-sealing faults. Engelder (1974) studied the relationship between cataclasis and the formation of fault gouge. The existence and distribution range of fault gouges were then confirmed using the ring-shear test by Weber et al. (1978). Through field observations and sample tests, Smith (1980) showed the strong sealing ability of the shale smear layer. Downey (1984) pointed out that the fault sealing properties should be considered as vertical sealing and lateral sealing.

Based on these research studies, Bouvier et al. (1989) came up with the concept of clay smear potential (CSP) and the calculating method. Lindsay et al. (1993) used the shale smear factor (SSF) to calculate the fault sealing property quantitatively. During this

period, Allan (1989) proposed a conceptual model to study the state of sand–clay docking between two fault plates using the cross-sectional profile graphical method based on the theoretical basis of sand–clay docking sealing.

Quantitative evaluation of the fault sealing property started to be put into practice in 1996 (Lyu et al., 1996). Yielding et al. (1997) started to evaluate fault sealing quantitatively by calculating the shale gouge ratio (SGR). After Yielding's attempt, there were more and more articles on the quantitative evaluation of fault sealing and its related parameters. Bretan et al. (2003) pointed out that the SGR can be used to estimate the maximum hydrocarbon column height supported by faults based on sorting a large amount of fault data worldwide. Lyu et al. (2009) considered using the displacement pressure contrast of fault rock against a reservoir to evaluate the fault lateral sealing property quantitatively.

In recent years, an increasing number of scholars have adopted a comprehensive research approach to investigate fault sealing. Wang et al. (2019) undertook an integrative study using core, wireline logs, and seismic data to analyze the architecture of reservoirs and seals of the Lower Jurassic System in the Surat Basin. He et al. (2021) studied the variability in fault reactivation models according to differences in fault throw potential influences across-fault juxtaposition of strata and sealing potential for CO_2 storage of overlying strata in the Surat Basin. The study provides a framework to understand fault architecture and predict which parts of the basin are more prone to the juxtaposition of strata forming transmissive versus sealing relationships. Peng et al. (2021) discussed the evolution, sealing, and damage mechanism of the normal fault in the Yanchang Formation of the Jinhe oilfield, Ordos Basin, based on a series of physical simulation experiments and the particle image velocimetry (PIV) technique.

A series of geotectonic features have been studied in the Lishui Sag. Based on the analyses of gravity and magnetic data by Ma et al. (2018) and Jiang et al. (2019), it is considered that the main control faults in the Lishui Sag are NE–SW trending. Inside the sag, multiple sets of strike-slip faults with nearly east–west strikes have developed. The existence of this series of faults divides the sag into several small sub-sags. Wang et al. (2000), Yang and Wang (2002), and Zhang et al. (2014a) made a comprehensive discussion on the extension characteristics of the Lishui Sag through various technical means such as balanced section technology and pointed out that there are some differences in the extension of different regions and different geological stages in the sag. In the late Cretaceous–Paleocene stage, the extension of the sag was dominated by the multi-stage and progressive "curtain" horizontal extension. At the same time, in the fault depression period, due to the influence of tensile stress, a series of normal faults appeared. The lateral distance of normal faults and a tilt in block faults appeared. The early Lishui fault depression basin is mainly composed of small and relatively independent fault depressions. Based on geological and seismic data on the Lishui Sag, scholars have identified the main petroleum geological conditions in the sag. However, due to its complex structural features, rich structural styles, and complex sedimentary distribution, few studies have examined the hydrocarbon migration channels and transportation systems, which has affected the prediction and evaluation of hydrocarbon resources in the Lishui Sag.

Regional geologic setting

Located in the southwestern part of the East China Sea Shelf Basin, the Lishui Sag is a part of the Taipei Depression. The Lishui Sag is distributed in a NE–SW striking, on the east of the Minzhe Uplift. The Yandang Uplift is on the east of the Lishui Sag, while the Jiaojiang Sag is on the north. The area of the Lishui Sag is about 15,000 square kilometers, and the maximum sedimentary thickness is about 15,000 m (Figure 1).

The Lishui Sag is a Cenozoic rift basin formed of Mesozoic residual basins. Controlled by the NE–SW trending faults, the Lishui Sag developed with a typical "east-fault and west-overlap" feature. The whole sag can be divided into northern and southern sections, while the different tectonic appearances show between the west and east zones. The west part of the Lishui West Sag connects with the Minzhe Uplift by a gentle slope zone, while the east part connects with the Lingfeng Uplift through edge faults of the steep slope zone. The Lishui East Sag also presents the structural characteristics of the western gentle slope zone and eastern steep slope zone. The Lishui Sag has experienced three tectonic evolution stages: the syn-rift stage (the Yueguifeng Formation and Lingfeng Formation in Pliocene), transition stage (the Mingyuefeng Formation in Pliocene), and post-rift stage (after Eocene). The Cenozoic strata from bottom to top are the lower Paleocene Yueguifeng Formation (E_1y), the upper Paleocene Lingfeng Formation (E_1l), the Mingyuefeng Formation (E_1m), the lower Eocene Oujiang Formation (E_2o), the middle Eocene Wenzhou Formation (E_2w), and Miocene, Pliocene, and the Quaternary. The upper Eocene and the Oligocene strata are missing (Figure 2). As the vital exploration target area, the area of the Lishui West Sag is about 6,900 km^2, and the upper Paleozoic Lingfeng Formation and the Mingyuefeng Formation are the primary exploration target intervals.

The China National Offshore Oil Corporation, Primeline Energy Holdings Inc., and many other companies have carried out a series of hydrocarbon explorations in the Lishui Sag since the 1970s. The exploration discovered the L Gas Field and gained a large number of seismic data and log data (Ge et al., 2019). However, the exploration work has been stagnant, and no breakthroughs have been made since the discovery of the L Gas Field at the end of the last century (Cui and Zhao, 2015; Zhong et al., 2018).

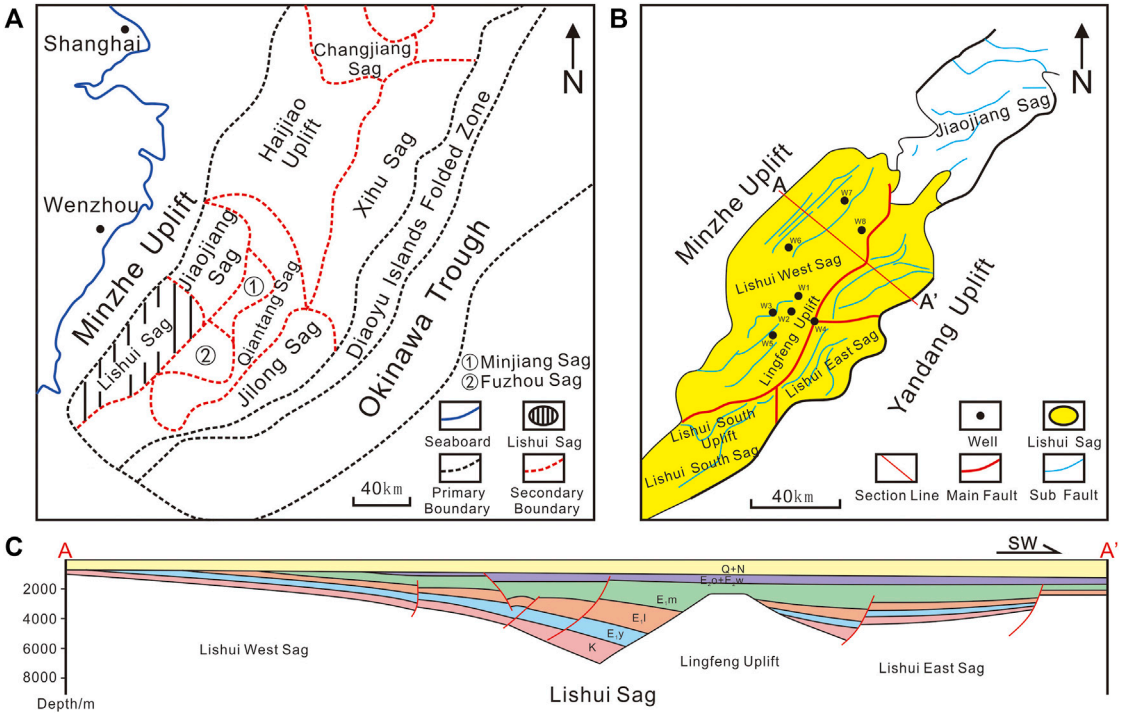

FIGURE 1
Regional geologic setting of the Lishui Sag. **(A)** The Lishui Sag, located in the west–south part of the East China Sea Basin, on the west of the Yandang Uplift, east of the Minzhe Uplift, and south of the Jiaojiang Sag. **(B)** Lishui Sag, containing five tectonic units. The extension causes a series of NE- to NNE-striking normal faults in this area. **(C)** Geological section, showing the basic tectonic features in the Lishui Sag.

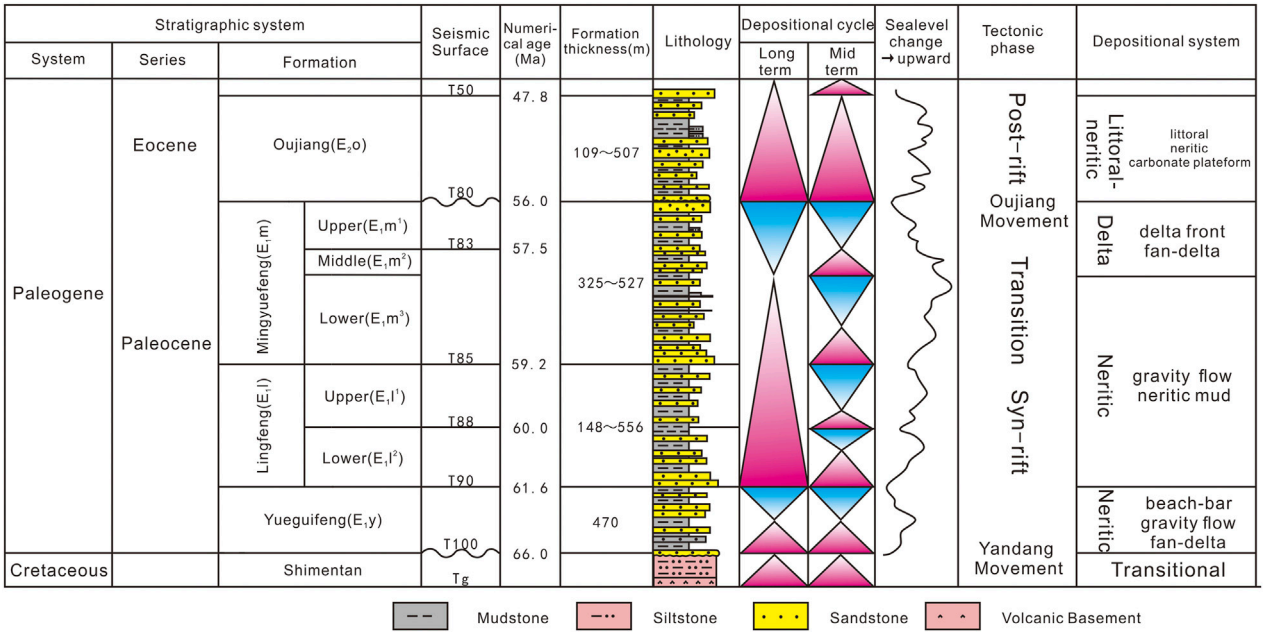

FIGURE 2
Comprehensive histogram of early Paleogene in the Lishui Sag.

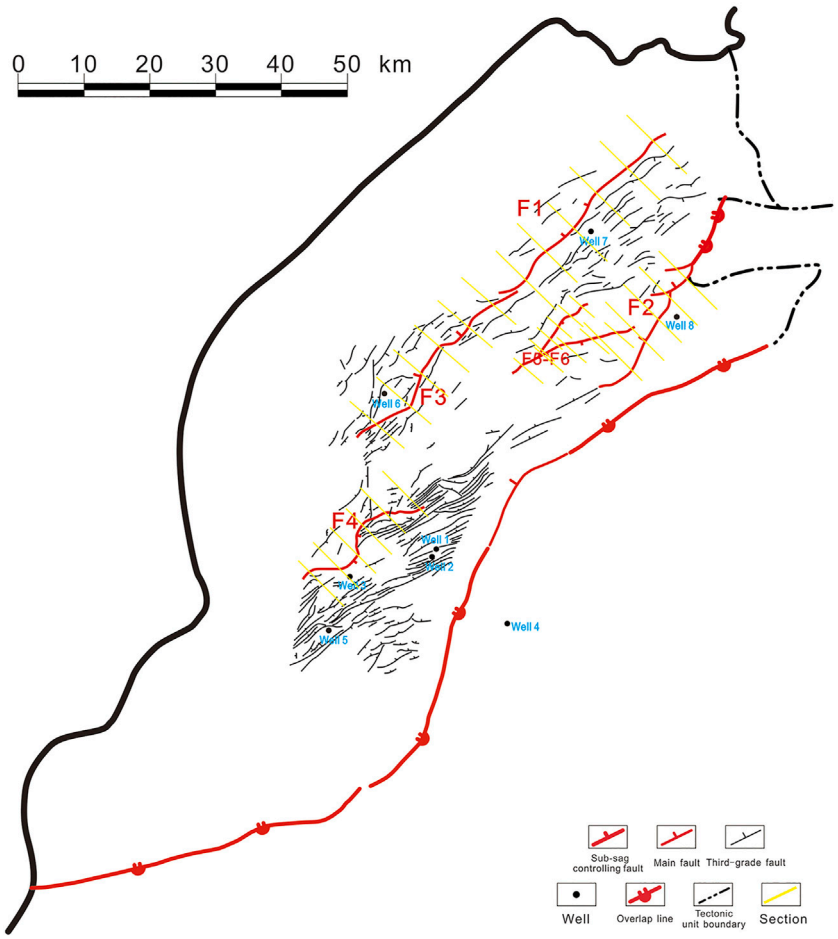

FIGURE 3
Fault system of the T90 reflector in the Lishui West Sag.

Methodology

Fault activity

The seismic data on the Lishui West Sag show that 135 faults developed in the Pliocene strata, including six main faults (Figure 3). There are 26 faults in the north, 23 faults in the middle transfer zone, 33 faults in the southeast area (L block), 25 faults in the south depression zone, and 28 faults in the south slope zone (the western gentle slope zone), and all faults are normal faults.

This study uses the fault activity rate (V) method to calculate the fault activity intensity of all six main faults in the Lishui West Sag. Based on the accuracy of the existing seismic profile interpretation results and the practical demand for Paleocene hydrocarbon research, a series of deposition periods are selected. There are faults F1, F2, F3, F5, and F6 in the northern section, while F4 is in the southern section. We chose K_2s, E_1y, E_1l^2, E_1l^1, E_1m, and E_2o+E_2w formations' deposition period to calculate the fault activity rate in the northern section. In the southern section, we chose K_2s+E_1y, E_1l^2, E_1l^1, E_1m^2+E_1m^3, E_1m^1, and E_2o+E_2w formations' deposition period to calculate the activity rate of fault F4.

Combined with the actual seismic and geological characteristics, the unit of the main fault activity rate in the Lishui West Sag is selected as a meter per million years (m/Ma). Based on the quality of seismic data, six section lines of faults F1, F3, and F4 were selected, and five section lines of faults F2, F5, and F6 were selected (Figure 3). According to the calculation results, we plotted the activity rate curves of six main faults corresponding to the deposition period. We quantitatively described the activity intensity of the main faults in the Lishui West Sag (Figure 4).

What can be seen from the evolution curve of V is that the main active periods of the main faults in the Lishui West Sag are in the range of the Paleocene (the rifting stage). Since the beginning of the Eocene, the intensity of the fault activity has been significantly reduced, while the Oligocene strata are absent in the Lishui West Sag. From Miocene to the Quaternary, the V of

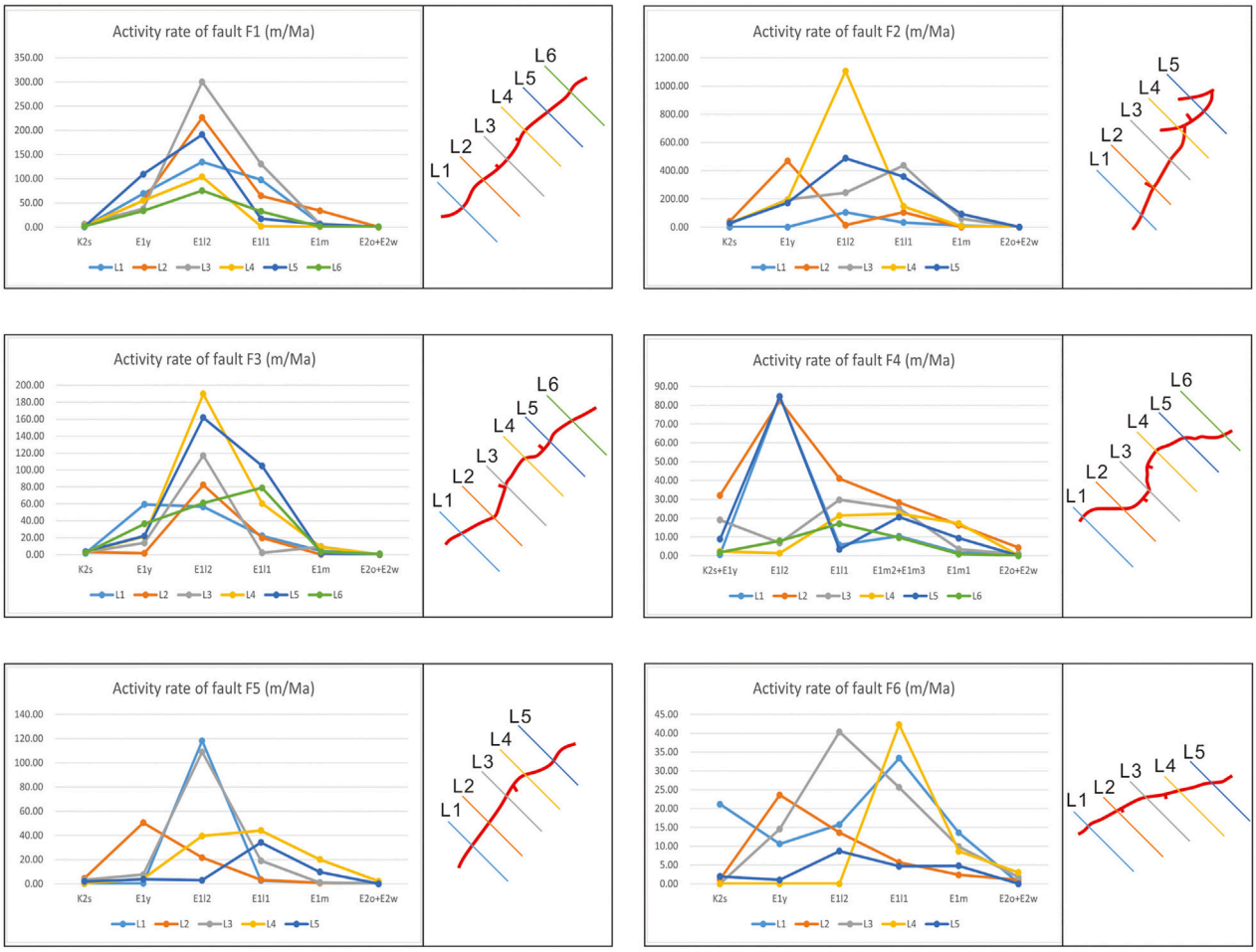

FIGURE 4
V of main boundary faults in the Lishui West Sag.

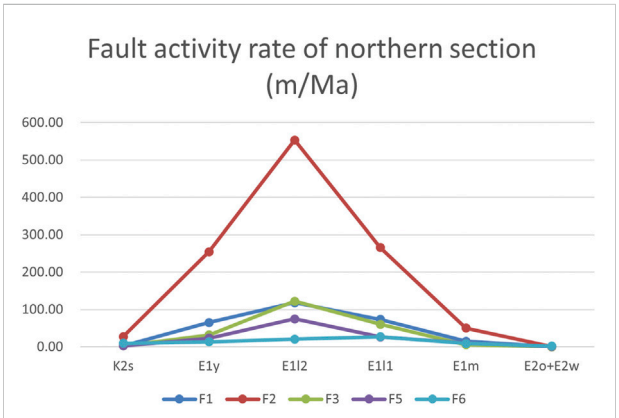

FIGURE 5
RMS V of main boundary faults of the northern section in the Lishui West Sag.

main faults in the Lishui West Sag is almost zero. In other words, the activity of the main faults in the Lishui West Sag stopped at that time.

In order to ensure the accuracy of the data and facilitate the comparison of the difference in the activity intensity of each main fault, the main faults in the southern section and the northern section are respectively processed by the root mean square (RMS) method (Figures 5, 6).

Data processing indicates that the main active period of the main fault in the west sub-depression of the Lishui Sag is from E_1y to E_1l. In the period of E_1l^2, the value of main faults reached the highest. In other words, during the E_1l, the fault rift in the Lishui West Sag reached its climax, meaning the regional tectonic activity in the Lishui West Sag had the most significant impact on terrain development during this period.

Among the value of RMS V in the northern section, we discovered that the V of fault F2 is higher than the others. The reason for this is the syn-deposition of fault F2 and the only sub-sag

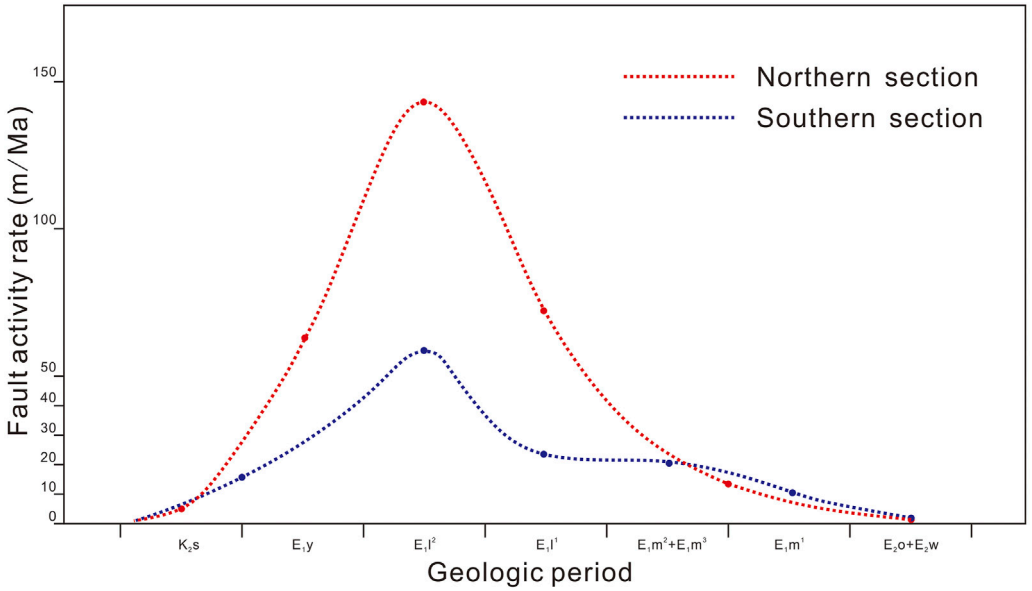

FIGURE 6
RMS V of main boundary faults of northern and southern sections in the Lishui West Sag.

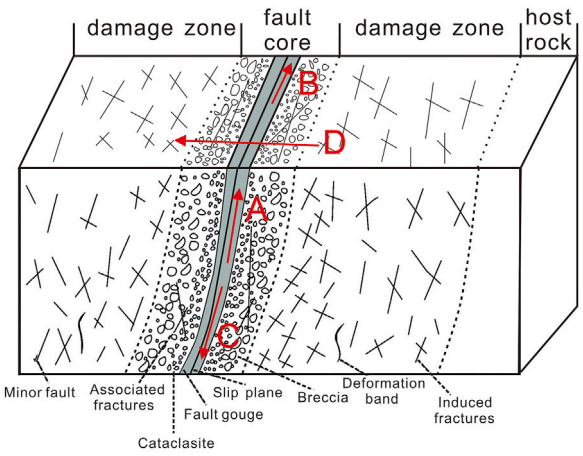

FIGURE 7
Different transporting forms of fault hydrocarbon transportation. **(A)** The vertical upward migration of hydrocarbon along the fault plane. **(B)** The migration of hydrocarbon along the fault strike. **(C)** The vertical downward migration of hydrocarbons along the fault plane. **(D)** The migration of hydrocarbon through the fault plane.

controlling fault in the Lishui West Sag. In the E_1l^2 period, the activity intensity of fault F2 was 26.74 times that of fault F6. Therefore, in the analysis of the active intensity of the main faults in the northern section of the Lishui West Sag, we removed data on fault F2 for statistics to ensure the accuracy of data on the active intensity of the northern main faults. After the removal operation, the activity intensity of the main faults in the northern section was weakened (Figure 6). However, the value of the northern section is still higher than that of the southern section. This shows that in this period, the comprehensive activity intensity of faults in the northern section was more vital than that in the southern section.

Furthermore, we note that the main faults in the southern section still have high activity in the late deposition period of E11, and that the fault activity intensity was further weakened after the transition stage (Figure 6).

Fault hydrocarbon transporting

The forms of hydrocarbon transportation related to faults can be divided into two types; one is along the fault plane (Figures 7A–C), and the other is through the fault plane (Figure 7D). The hydrocarbon transportation which forms along the fault plane can be divided into three types. The most important type is the vertical upward migration of hydrocarbon along the fault plane, which is often accompanied by the diffusion and migration of hydrocarbons across the fault plane on both sides. The second type is the form of hydrocarbon transportation along the fault strike, which has specific requirements for transportation conditions. First, the fault zone should maintain the advantages of transportation. Second, there are fluid potential differences or structural potential differences along the fault strike. The third is the sealing of the cap rock in the upper

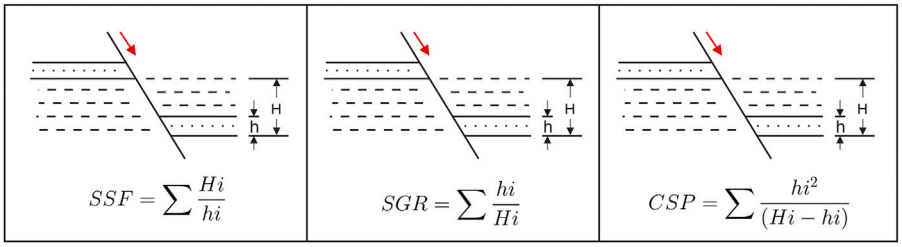

FIGURE 8
Quantitative methods of the shale smear.

part of the fault zone, so vertical upward transportation cannot be realized. The last type is the vertical downward migration of hydrocarbons along the fault plane.

This type of transportation requires that the downward abnormal pressure of the hydrocarbon source rock is much greater than the buoyancy, strata gradient force, and other vertical upward forces (Zha et al., 2002). At present, there are a large number of research examples of this kind of "Reversed Migration" reservoir, such as the Sanzhao Depression in the northern Songliao Basin, which proves the universality of this kind of hydrocarbon transportation form (Fu et al., 2009; Yu, 2021).

Results

Shale smear sealing

Combined with previous studies, we believe that three dimensions affect the fault zone transporting capacity under the cap rock of the Lishui West Sag. The first is the lithology configuration relationship of the fault zone in the Lishui West Sag, that is, the lithology juxtapositional sealing. The second is the influence of the sealing layer on the shale smearing mode in the Lishui West Sag; the third is the pressure-bearing mode of fault rock, that is, the pressure effect of the hydrocarbon-bearing system (Lei et al., 2019).

The caprock of the Lingfeng Formation in the Lishui West Sag is shale. Lindsay et al. (1993) believed that the shale smear factor (SSF) could quantitatively evaluate the sealing property of the caprock (Yielding et al., 2010). At the same time, there are also indicators such as the shale gouge ratio (SGR), shale smear potential (CSP), clay content ratio (CCR), and many other indicators to quantitatively analyze the smear effect of shale caprock (Downey, 1984; Yielding et al., 1997; Yielding et al., 1999; Zhang et al., 2014b) (Figure 8).

Macroscopically, the shale caprock of the Lingfeng Formation in the Lishui West Sag has prominent sectional characteristics: the upper Lingfeng Formation (E_1l^1) is mainly thick shale; the lower Lingfeng Formation (E_1l^2) shows the characteristics of multi-group thin sediment stack and sand-mud interbeds in the vertical sedimentary sequence. Liu and Li (2015), through physical simulation, found that the number of shale layers in the caprock has a significant influence on the deformation characteristics of shale. When the thickness of shale and sandstone is uniform, there are more layers of shale, and the smearing effect of the shale appears to be worse. For single-layer shales, the greater the thickness and depth of the shale, the stronger the smearing effect appears (Lyu et al., 2000).

Based on existing data on the study area, this study calculates the main characterization parameters related to the shale sealing of the main faults (Table 1). The rock lithology and thickness of the four main faults F1–F4 (F5 and F6 data missing) from the lower Lingfeng Formation to the Mingyuefeng Formation are clarified and statistically analyzed combined with logging data.

Fault lateral sealing

When the fault is in the active stage, the lateral hydrocarbon transport of the fault zone is not apparent. When the fault is in a relatively static stage, the lateral hydrocarbon transportation of the fault zone depends mainly on the juxtapositional sealing of lithology. The lithology juxtapositional sealing rate(e)of a specific stratum is equal to the ratio of the total thickness of unconnected sandstone to the total thickness of sandstone. The e value is negatively correlated with the hydrocarbon transportation effect, but it is challenging to carry out practical statistics in exploration and development practice (Figure 9).

We collected the published data on the sand ratio and lithology juxtapositional sealing rate in Daqing, Liaohe, and many other oilfields (Table 2). These data show a specific relationship between the sand ratio and the lithology juxtapositional sealing rate, so we use the mathematical method to fit the formula (Lyu et al., 1996).

Based on the collected data, we fitted and obtained the empirical formula of the lithology juxtapositional sealing rate:

$$e = -38.79\,ln(\sigma) + 5.4405.$$

In this formula, e denotes the lithology juxtapositional sealing rate, dimensionless, and σ denotes the formation sand ratio, dimensionless. R^2=0.7076 after fitting the formula shows a

TABLE 1 Shale smear of main faults in the Lishui West Sag.

Fault	Formation	Strata thickness(m)	Shale layer	SSF	SGR	CSP	Remark
F1	E1m	695	68	5.29	0.19	0.23	
	E1l1	409	44	5.35	0.19	0.23	
	E1l2	427.8	50	5.98	0.17	0.20	
F2	E1m	442	60	3.52	0.28	0.40	
	E1l1	165	30	1.74	0.58	1.36	
	E1l2	*					No data
F3	E1m	437	28	2.08	0.48	0.92	
	E1l1	259	23	3.42	0.29	0.41	
	E1l2	384	40	2.50	0.40	0.67	
F4	E1m	951	73	3.01	0.33	0.50	
	E1l1	267	20	5.40	0.19	0.23	
	E1l2	*					No data

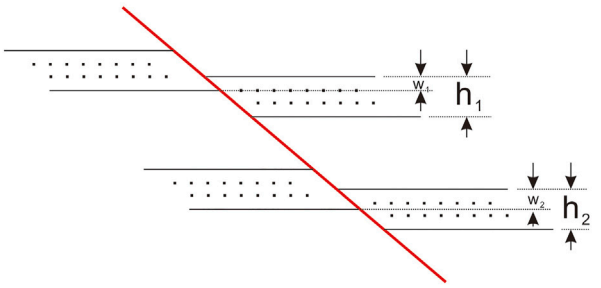

FIGURE 9
Definition of the lithology juxtapositional sealing rate (e). $e = \sum \frac{hi-wi}{hi}$.

TABLE 2 Published data on similar basins in East China.

No.	Facies	Sand ratio	e (%)
1	Fluvial	0.205	48.1
2	Fluvial	0.185	73.2
3	Fluvial	0.105	91.5
4	Fluvial	0.165	85.4
5	Delta	0.49	26.6
6	Delta	0.28	49.3
7	Fluvial	0.33	72
8	Delta	0.385	38.8

corresponding good relationship. Therefore, we can use this method to connect the sand ratio with the connectivity efficiency to deduce the approximate effect of the lateral sealing of the fault and approximately describe the lateral sealing of the fault according to the characteristics of the insufficient data on the Lishui West Sag.

TABLE 3 Lithology juxtapositional sealing rate (e) of main faults in the Lishui West Sag.

Fault	Formation	Depth(m)	Sand ratio	e (%)
F1	E_1m	2,936	0.19	69.86
	E_1l^1	3,345	0.19	69.86
	E_1l^2	3,772.8	0.17	74.17
F2	E_1m	2,761	0.28	54.82
	E_1l^1	2,926	0.58	26.57
	E_1l^2	*		No data
F3	E_1m	1761	0.48	33.91
	E_1l^1	2020	0.29	53.46
	E_1l^2	2,404	0.40	40.98
F4	E_1m	2,641	0.33	48.45
	E_1l^1	2,908	0.19	69.86
	E_1l^2	*		No data

Based on the empirical formula of the lithology juxtapositional sealing rate, we calculated the lateral fault sealing of faults F1–F4, and the results are shown in Table 3:

Fault vertical sealing

The vertical sealing of the fault is mainly indirectly controlled by the fault plane's normal pressure. Furthermore, the fault plane normal pressure directly controls the diagenetic degree of the fractured fragments, such as the fault rock on the fault plane. Ultimately, the diagenetic degree of fractured fragments directly determines the displacement pressure. Therefore, the displacement pressure (Pd) at the fault plane can be used to quantitatively characterize the vertical sealing of the fault. The greater the fault displacement pressure, the worse the vertical fault sealing (Lyu et al., 2007).

Zhang et al. (2014b) came up with the concept of the vertical shale smear evaluation parameter (Q) of the main faults in 2014.

With this parameter, we can quantitatively evaluate the vertical sealing of growing faults. The relationship between the vertical shale smear coefficient (Q) and the shale gouge ratio (SGR) is expressed as follows:

$$Q = \frac{P_1}{P_1 - P_2} \times SGR.$$

In this formula, P_1 is the fault plane normal pressure, MPa; P_2 is the fracture pressure of shale, MPa; SGR is the shale gouge ratio, dimensionless; and Q is the vertical shale smear coefficient, dimensionless.

In this formula, the greater the fault plane normal pressure, the greater the vertical shale smear coefficient Q, and the stronger the vertical fault sealing. The more significant the difference between the fault plane normal pressure and the fracture pressure of shale, the weaker the smearing ability of the shale, and the weaker the vertical sealing of the fault.

According to the obtained SRG of the main faults in the Lishui West Sag (Table 1), we calculate the fracture pressure of the shale by Eaton's method (Eaton, 1969), and the calculation expression is as follows:

$$P_2 = G_f \times D = \left[\frac{v}{1-v}(G_b - G) + G\right] \times D.$$

In this formula, P_2 is the fracture pressure of the shale, MPa; G_f is the fracture pressure gradient of the shale, MPa/m; D is the depth, m; v is the Poisson ratio, dimensionless; G_b is the pressure gradient of overlying strata, MPa/m; and G is the pore fluid pressure gradient of strata, MPa/m.

Based on previous research studies (Fu et al., 2003; Lyu et al., 2007; Lyu and Wang, 2010; Tan et al., 2018; Li et al., 2020), we conclude that the fault plane's normal pressure is the component of the strata on the fault plane, indicating that the fault plane normal pressure of the main faults in the Lishui West Sag is

$$P_1 = 0.009876(\rho - \rho_w)\cos\theta D.$$

In this formula, P_1 is the fault plane's normal pressure, MPa; ρ is the average density of overlying strata, g/cm^3; ρ_w is the density of strata water, g/cm^2; θ is the dip of the fault plane; and D is the breaking point depth, m.

By referring to the related parameters of similar faults in adjacent areas (Xiang, 2008; Xie et al., 2021; Zhao et al., 2021; He et al., 2022), aiming at the fault development in the Lishui West Sag, we assigned a Poisson ratio of 2.0. We used the hydrostatic column pressure gradient instead of the pore fluid pressure gradient, G=0.0107 MPa/m; and the average pressure gradient instead of the overlaying pressure gradient, Gb =0.0231 MPa/m. Through conversion, the average density of overlaying formation can be obtained as 2.357 g/cm^3. The density of strata water of the Lishui West Sag is 1.092 g/cm^3.

The fracture pressure of the shale of the main faults F1–F4 in the Lishui West Sag is calculated by referring to the aforementioned formula and index parameters. Because the fault plane normal pressure is not equal everywhere, to keep the relative rationality of the results and the value of the relative consistency, the fault dip angle was calculated using the average dip angle of the selected sections of the main faults in this study. Based on the horizontal–vertical proportional relationship of the profile, we increased the proportional coefficient r = 2.2 to correct the data results.

According to the calculation results of P1, P2, and SGR, we further calculated the vertical shale smear evaluation parameter (Q) of the main faults F1–F4 in the Lishui West Sag. The calculation results are shown in Table 4:

TABLE 4 Vertical shale smear evaluation parameter (Q) of the main faults in the Lishui West Sag.

Fault	Formation	P_1 (MPa)	P_2 (MPa)	SGR	Q
F1	E_1m	53.08	40.52	0.19	0.25
	E_1l^1	63.72	46.16	0.19	0.26
	E_1l^2	56.03	52.06	0.17	0.18
F2	E_1m	61.93	38.10	0.28	0.46
	E_1l^1	72.67	40.38	0.58	1.04
	E_1l^2	*			No data
F3	E_1m	49.51	24.30	0.48	0.98
	E_1l^1	50.90	27.88	0.29	0.53
	E_1l^2	60.57	33.18	0.40	0.73
F4	E_1m	60.05	36.45	0.33	0.55
	E_1l^1	69.55	40.13	0.19	0.32
	E_1l^2	*			No data

Discussion

Shale smear sealing

From the calculation results in Table 1, it can be concluded that the layer number of shale strata in E_1l^1 of each main fault is relatively tiny. However, the thickness is relatively large, indicating that the sealing ability is better than the overlying strata. This shows that the smearing effect of the shale caprock in E_1l^1 is strong and the sealing effect of hydrocarbon transportation is better in E_1l^1. The abnormal characteristics of fault F2 may be due to the lack of data collection of E_1l^2 and part of E_1l^1. Other possible reasons are that fault F2 is located in the steep slope zone, the geological structure is relatively complex, and the mutation is strongly correlated.

Fault lateral sealing

From the data analyses in Table 3, it can be concluded that among all the main faults, the lateral sealing of the main fault

F1 is the best, followed by F4 and F3. In the E_1l period, the lateral sealing of fault F2 was the worst, which reflected that F2 was an extension fault of the regional control fault to some extent. During the E_1l period, the scale of the activity intensity of F2 was significantly stronger than that of other main faults, which was extraordinary.

In the longitudinal time series, the lateral sealing of the E_1l period of faults F1, F3, and F4 is stronger than that of the E_1m period, indicating the critical influence of lithology difference on the lateral sealing of faults. This is typical in the longitudinal comparison of fault F3. Large sets of thick shale developed in the E_1l^1 period of fault F3 and its lateral sealing property is better than that of the underlying E_1l^2 and the overlying E_1m.

We also note that fault F1 in the E_1l period has no apparent advantage in the lateral sealing of E_1m. The lateral sealing of fault F2 in the E_1l period is worse than that of the E_1m period. These phenomena, to some extent, reflect the weakening effect of the fault activity intensity on fault lateral sealing during this period. Based on this assumption, we can reasonably explain why the fault activity intensity of fault F2 in the E_1l period is significantly stronger than that of fault F1 and other faults. The lateral sealing of the main faults in the Lishui West Sag is ranked as F1 > F4 > F2 > F3.

Fault vertical sealing

The results in Table 4 show that the Q of the main faults in the Lishui West Sag is almost less than 1.0. The maximum value appears at 1.04 of E_1l^1 on fault F2, and the minimum value appears at 0.1 of E_1l^2 on fault F1. It indicates that the vertical sealing of the fault is not strong in general and has relatively good vertical hydrocarbon transportation capacity. The main faults are the possible dominant channels for hydrocarbon migration.

From the point of view of the time series, the vertical sealing of the E_1m period is better than that of the E_1l period, reflecting a more vital tectonic activity of the E_1l. The open faults are conducive to hydrocarbon transportation and migration at that time. From the perspective of spatial distribution, the vertical sealing property of fault F3 near the structural transfer zone of the Lishui West Sag is relatively good, while the vertical sealing of fault F1 in the western slope zone of the northern section is the worst. The overall vertical sealing property of the main faults in the Lishui West Sag is in the order of F3 > F2 > F4 > F1 from good to poor, which is precisely the opposite of the lateral sealing property of the main faults.

Conclusions

(1) Through the calculation of the relevant parameters of shale smear, our findings indicate that the shale caprock of the Lingfeng Formation in the Lishui West Sag has a strong smear effect and that the sealing effect of hydrocarbon transportation is better, which is helpful for the occurrence of hydrocarbons in the Lishui West Sag.

(2) The sealing ability of the main fault in the Lishui West Sag was quantitatively calculated. The shale filling of the fault helps enhance the lateral sealing ability of the fault, and the activity of the fault will weaken the lateral sealing ability of the fault. The activity intensity of the fault has a positive control effect on the vertical sealing ability of the fault, and the shale filling of the fault can weaken the influence of the fault activity intensity.

(3) The vertical sealing order and the lateral sealing order of the main faults in the Lishui West Sag are precisely the opposite, indicating that there is a specific negative correlation between the vertical sealing ability dominated by the fault activity intensity and the lateral sealing ability dominated by the fault shale filling, and the relationship between them needs to be further explored.

Data availability statement

The original contributions presented in the study are included in the article/supplementary material; further inquiries can be directed to the corresponding author.

Author contributions

BY processed data and wrote the manuscript. QF, JL, and WM provided funding and helped with the conception of the idea. BY compiled the data, drew plots, and edited the manuscript. SZ contributed to the conception, and reviewed and edited the manuscript. QF contributed to data processing and participated in discussion. QF reviewed and edited the manuscript.

Funding

This work is supported by the CNOOC seven-year action plan project (Grant No. CCL2020SHPS023RSI).

Conflict of interest

Authors JL and WM are employed by the Shanghai Branch Company of CNOOC (China) Ltd.

The remaining authors declare that the research was conducted in the absence of any commercial or financial relationships that could be construed as a potential conflict of interest.

Publisher's note

References

Allan, U. S. (1989). Model for hydrocarbon migration and entrapment within faulted structures[J]. *AAPG Bull.* 73 (07), 803–811.

Bouvier, J., Kaars-Sijpesteijn, C., Kluesner, D., Onyejekwe, C., and Van Der Pal, R. (1989). Three-dimensional seismic interpretation and fault sealing investigations, Nun River Field, Nigeria[J]. *AAPG Bull.* 73 (11), 1397–1414. doi:10.1306/44B4AA5A-170A-11D7-8645000102C1865D

Bretan, P., Yielding, G., and Jones, H. (2003). Using calibrated shale gouge ratio to estimate hydrocarbon column heights. *Am. Assoc. Pet. Geol. Bull.* 87 (03), 397–413. doi:10.1306/08010201128

Cui, M., and Zhao, Z. (2015). Constraint analysis of Lishui sag hydrocarbon accumulation in donghai basin[J]. *Special Oil Gas Reservoirs* 22 (02), 18–21+151.

Downey, M. W. (1984). Evaluating seals for hydrocarbon accumulations[J]. *AAPG Bull.* 68 (11), 1752–1763.

Eaton, B. A. (1969). Fracture gradient prediction and its application in oilfield operations. *J. petroleum Technol.* 21 (10), 1353–1360. doi:10.2118/2163-pa

Engelder, J. T. (1974). Cataclasis and the generation of fault gouge. *Geol. Soc. Am. Bull.* 85 (10), 1515–1522. doi:10.1130/0016-7606(1974)85<1515:catgof>2.0.co;2

Fu, G., Lyu, Y., Ma, F., and Fu, X. (2003). Comprehensive evaluation method for vertical sealing of fault and its application[J]. *Xinjiang Pet. Geol.* (05), 451–454.

Fu, X., Ping, G., Fan, R., and Liu, Z. (2009). Research on migration and accumulation mechanism of hydrocarbon "reversed migration" in fuyu and yangdachengzi Formation in Sanzhao depression[J]. *Acta Sedimentol. Sin.* 27 (03), 558–566.

Ge, H., Gao, S., Zhou, P., and Diao, H. (2019). Fault structural characteristics and its petroleum geological significance of Lishui sag in donghai basin[J]. *Adv. Geosciences* 9 (11), 1025–1035.

He, J., La Croix, A. D., Gonzalez, S., Pearce, J., Ding, W., Underschultz, J. R., et al. (2021). Quantifying and modelling the effects of pre-existing basement faults on folding of overlying strata in the Surat Basin, Australia: Implications for fault seal potential. *J. Petroleum Sci. Eng.* 198, 108207. doi:10.1016/j.petrol.2020.108207

He, Y., Zheng, J., and Zhang, M. (2022). Calculation method and application of formation fracture pressure in Baiyun deepwater area[J]. *Mar. Geol. Front.* 38 (05), 41–50.

Jiang, Z., Ming, Y., and Yao, G. (2019). Study on fault division of Lishui sag in East China Sea basin[J]. *Prog. Geophys.* 34 (01), 310–315.

Lei, Z., Xu, H., Liu, Q., Li, W., Yan, D., Li, S., et al. (2019). The influence of multiple-stage oil emplacement on deeply buried marine sandstone diagenesis: A case study on the devonian donghe sandstones, tabei Uplift, tarim basin, NW China. *Mar. Petroleum Geol.* 110 (C), 299–316. doi:10.1016/j.marpetgeo.2019.07.030

Li, H., Wu, J., Huang, J., Wang, Y., and Li, Z. (2020). Quantitative analysis of fault vertical sealing ability and its application in an oil field of Bohai Bay Basin[J]. *Bull. Geol. Sci. Technol.* 39 (04), 125–131.

Lindsay, N., Murphy, F., Walsh, J., and Watterson, J. (1993). Outcrop studies of shale smears on fault surfaces[J]. *Geol. Model. hydrocarbon reservoirs outcrop analogues* 15, 113–123.

Liu, X., and Li, H. (2015). Physical simulation of clay layer effect on clay smear and evolution [J]. *Fault-Block Oil and Gas Field.* 22 (06), 722–728. doi:10.6056/dkyqt201506009

Lyu, Y., Huang, J., Fu, G., and Fu, X. (2009). Quantitative study on fault sealing ability in sandstone and mudstone thin interbed[J]. *Acta Pet. Sin.* 30 (06), 824–829.

Lyu, Y., Li, G., Wang, Y., and Song, G. (1996). Quantitative analyses in fault sealing properties[J]. *Acta Pet. Sin.* (03), 39–45.

Lyu, Y., Sha, Z., Fu, X., and Fu, G. (2007). Quantitative evaluation method for fault vertical sealing ability and its application[J]. *Acta Pet. Sin.* (05), 34–38.

Lyu, Y., and Wang, S. (2010). Quantitative evaluation of fault seal[J]. *J. Northeast Petroleum Univ.* 34 (05), 35–41+166.

Lyu, Y., Zhang, S., and Wang, Y. (2000). Research of quantitative relations between sealing ability and thickness of cap rock[J]. *Acta Pet. Sin.* (02), 27–30+4.

Ma, G., Ming, Y., and Huang, D. (2018). Distribution characteristics study of cenozoic basement of lishui-jiaojiang sag based on gravity and magnetic anomalies [J]. *J. Jilin University(Earth Sci. Edition)* 48 (05), 1493–1500.

Peng, X., Deng, H., He, J., Chen, H., and Zhang, Y. (2021). Research on the evolution and damage mechanism of normal fault based on physical simulation experiments and Particle image Velocimetry technique. *Energies* 14 (10), 2825. doi:10.3390/en14102825

Smith, D. A. (1980). Sealing and nonsealing faults in Louisiana Gulf Coast salt basin[J]. *AAPG Bull.* 64 (02), 145–172.

Smith, D. A. (1966). Theoretical considerations of sealing and non-sealing faults [J]. *AAPG Bull.* 50 (02), 363–374.

Tan, L., Xie, H., Zhang, H., Zhao, J., and Guo, Y. (2018). A quantitative research method on the sealing of growth faults: A case study of JX1-1 oil field in liaozhong sag, Liaohe depression[J]. *Petroleum Geol. Exp.* 40 (02), 268–273.

Wang, J., La Croix, A. D., Gonzalez, S., He, J., and Underschultz, J. (2019). Sequence stratigraphic analysis of the lower jurassic precipice sandstone and evergreen Formation in the Surat Basin, Australia: Implications for the architecture of reservoirs and seals for CO_2 storage[J]. *Mar. Petroleum Geol.* 102, 829–843. doi:10.1016/j.marpetgeo.2019.01.038

Wang, Y., Jiang, L., and Yang, W. (2000). Kinematical analysis on faults in the Lishui Jiaojiang sag[J]. *Sci. Geol. Sin.* (04), 441–448.

Weber, K., Mandl, G., Pilaar, W., Lehner, F., Precious, R., et al. (1978). "The role of faults in hydrocarbon migration and trapping in Nigerian growth fault structures [C]," in Offshore Technology Conference. doi:10.4043/3356-ms

Xiang, L. (2008). Quantitatively analyze the main controlling factors of mudstone fracture in Jiyang Depression[J]. *Petroleum Geol. Recovery Effic.* (05), 31–33+37+113.

Xie, J., Wu, H., Lou, Y., and Zhai, Y. (2021). Fracture pressure prediction model of high temperature and high-pressure formation in deep water area of the South China Sea[J]. *Fault-Block Oil Gas Field* 28 (03), 378–382.

Yang, W., and Wang, Y. (2002). The analysis of the basin's extension in the Lishui Jiaojiang Sag[J]. *J. Southwest Petroleum Inst.* (03), 8–10+5.

Yielding, G., Bretan, P., and Freeman, B. (2010). fault seal calibration: A brief review. *Geol. Soc. Lond. Spec. Publ.* 347 (01), 243–255. doi:10.1144/sp347.14

Yielding, G., Freeman, B., and Needham, D. T. (1997). Quantitative fault seal prediction[J]. *AAPG Bull.* 81 (06), 897–917.

Yielding, G., Øverland, J., and Byberg, G. (1999). Characterization of fault zones for reservoir modeling: An example from the Gullfaks field, northern North Sea[J]. *AAPG Bull.* 83 (06), 925–951.

Yu, Y. (2021). Predicting method of migration and accumulation space of the hydrocarbon reversed in upper source-lower reservoir combination and its application[J]. *Petroleum Geol. Oilfield Dev. Daqing* 40 (06), 44–51.

Zha, M., Qu, J., and Zhang, W. (2002). The relationship between overpressure and reservoir forming mechanism[J]. *Petroleum Explor. Dev.* (01), 19–23.

Zhang, T., Zhang, J., Zhang, S., Yu, Y., Tang, X., et al. (2014). An application of the balanced cross-section technique: The tectonic evolution of Lishui sag, the east China Sea Shelf basin[J]. *Shanghai Land & Resour.* 35 (01), 92–96.

Zhang, W., Zhang, W., and Zhang, Q. (2014). An improved method of shale smear evaluation[J]. *Xinjiang Oil Gas* 10 (01), 19–22+4.

Zhao, L., Liu, J., Yao, Y., Zhong, K., Ma, J., Zou, C., et al. (2021). Quantitative seismic characterization of source rocks in lacustrine depositional setting using the Random Forest method: An example from the Changjiang sag in East China Sea basin[J]. *Chin. J. Geophys.* 64 (02), 700–715.

Zhong, K., Zhu, W., Gao, S., and Fu, X. (2018). Key geological questions of the formation and evolution and hydrocarbon accumulation of the east China Sea Shelf basin[J]. *Earth Sci.* 43 (10), 3485–3497.